frontiers | Frontiers in Materials

TYPE Original Research
PUBLISHED 27 June 2025
DOI 10.3389/fmats.2025.1612050

OPEN ACCESS

EDITED BY
Changtai Zhou,
City University of Hong Kong, Hong Kong, China

REVIEWED BY
Meiben Gao,
Xihua University, China
Zhiguo Lu,
State Key Laboratory of Intelligent Coal Mining and Strata Control, China
Aibing JIn,
University of Science and Technology Beijing, China
Chunwang Zhang,
Taiyuan University of Technology, China
Chunde Piao,
China University of Mining and Technology, China

*CORRESPONDENCE
Sun Yao,
21403020407@stu.xust.edu.cn

RECEIVED 15 April 2025
ACCEPTED 13 June 2025
PUBLISHED 27 June 2025

CITATION
Shuai Z, Yao S, Jiantao C, Xingping L and Longquan W (2025) Research and optimization on the strength recovery mechanism of post peak fragmentation grouting reinforcement in mining rock mass. *Front. Mater.* 12:1612050.
doi: 10.3389/fmats.2025.1612050

Research and optimization on the strength recovery mechanism of post peak fragmentation grouting reinforcement in mining rock mass

Zhang Shuai[1,2], Sun Yao[1]*, Cao Jiantao[1,2], Lai Xingping[1,2] and Wu Longquan[1]

[1]College of Energy Science and Engineering, Xi'an University of Science and Technology, Xi'an, Shaanxi, China, [2]Key Laboratory of Western Mines and Hazard Prevention of China Ministry of Education, Xi'an University of Science and Technology, Xi'an, Shaanxi, China

To reveal the strength recovery characteristics of grout-reinforced engineering rock masses, this study is based on the small coal pillar god-side entry of the Maiduo Mountain Coal Mine. Uniaxial compression tests were conducted on grout-consolidated samples, complete surrounding rock samples, and grout-reinforced samples of post-peak broken surrounding rock. The mechanical properties of grout-consolidated samples of four grouting materials, as well as the strength recovery characteristics, crack propagation, and energy evolution of grout-reinforced post-peak fractured rock samples with different consolidation times were investigated. The results show that, compared to samples reinforced with ordinary cement, fly ash cement, and portland cement, the grout-consolidated samples made with high-performance cement-based materials exhibit the best strength recovery effect at any consolidation time, without significant pressure release or fluctuation during compression. Compared to the initial complete rock samples, the stress, strain, ring count, and cumulative energy of grout-reinforced post-peak fractured rock samples are significantly reduced, and they exhibit a notable linear positive correlation with consolidation time.

KEYWORDS

surrounding rock of roadway, post-peak fractured rock mass, grouting reinforcement, mechanical properties, strength recovery

1 Introduction

During the excavation of underground roadways, the bearing capacity of the surrounding rock has a significant impact on the stability of the roadway. Excavation-induced disturbances disrupt the original stress equilibrium, causing stress concentration in the surrounding rock. This leads to large deformations of the surrounding rock, roof collapse, floor heaving, spalling, and other engineering disasters (Guo et al., 2022; Xu et al., 2024; Zhang et al., 2022). Surrounding rock control technologies have progressively developed from passive support to active reinforcement and, ultimately, to integrated

modification methods. Grouting reinforcement, in particular, has proven highly effective in stabilizing fractured rock masses by filling discontinuities, enhancing integrity, and restoring load-bearing capacity (Kang, 2021; Kang et al., 2020; Qiu et al., 2025; Zhou et al., 2025). Insufficient strength recovery may lead to sustained deformation of surrounding rock, resulting in support system failure, ventilation difficulties, or disaster accidents, increasing maintenance and safety management costs. Therefore, research on the reinforcement effect of fractured surrounding rock is of great engineering significance.

Grouting reinforcement of the roadway surrounding rock is one of the effective methods for enhancing the integrity and bearing capacity of fractured surrounding rock, as well as preventing large deformations and leakage (Li et al., 2020; Zhang et al., 2023; Lu et al., 2022). Current research in surrounding rock reinforcement focuses on optimizing grouting materials, developing models for grout behavior, and integrating real-time monitoring technologies. These efforts are crucial for improving roadway stability, reducing maintenance costs, and enhancing safety in deep mining and tunneling environments (Huang et al., 2023; Lu et al.; Qilian et al., 2024; Liu et al.).

The intrinsic properties of grouting materials are crucial to the reinforcement effectiveness of surrounding rock. In response, the engineering community has developed a range of grouting materials for different projects (Lin et al., 2020; Mu et al., 2021; He et al., 2023). Cement-based grouting material has been widely studied due to its abundant source, strong impermeability, low cost, and good fluidity. However, high shrinkage limits its applicability in practical engineering projects (Shu et al., 2022; Wang et al., 2022; Pan et al., 2024; Oppong et al., 2023). To address this, some scholars have sought to improve the physical and mechanical properties of cement-based grouting material through the use of additives (Guo et al., 2020; Li et al., 2021; Cao and Yan, 2019). Regarding other grouting materials, Liu et al. (2020) developed a novel powdered grouting material (S-F powder geopolymer), which is prepared from slag powder, fly ash, alkaline activator A and B, chemical additives, reinforcing materials, and water. Zhang et al. (2019) proposed a low-cost, high-density grouting material for cracks in roadway floor slabs. Li et al. (2023) found that the dynamic compressive performance of cementitious composite materials incorporating carbon nanotubes (CNTs) and fly ash could be improved by 10.25%–31.86%. Ren et al. (2022) developed a new intelligent optimization method to determine the optimal mix ratio for cement grouting materials. Zhang et al., (2021) prepared alkali-activated slag/fly ash grouting materials using industrial waste as raw materials. Tan et al. (2019) further wet-milled slag powder to obtain ultra-fine grouting materials, enhancing the 28-day strength of cement-ground granulated blast furnace slag systems. These research findings have greatly enriched the variety of grouting materials and advanced the development of grouting technology.

The mechanical properties of rock masses reinforced with grouting materials have been widely studied (Tian et al., 2018; Qu et al., 2024; Liu et al., 2024). Lu et al. (2017) conducted grouting reinforcement of sandstone specimens containing abundant joints using cement grout. They used digital image correlation and acoustic emission monitoring techniques to investigate the acoustic emission characteristics during the loading and deformation process of the specimens before and after grouting reinforcement. The results showed that the acoustic emission activity of fractured specimens increased initially and then decreased with increasing filling ratio. Lee et al. (2000) conducted a comparative analysis based on numerical experiments and laboratory tests to evaluate the strength recovery of rock masses containing jointed fissures after grouting reinforcement. They proposed an inversion analysis method for quantitatively assessing the strength recovery effect of grouted rock masses. Sang et al. (2024) performed direct shear tests on mudstone specimens with fissures before and after grouting reinforcement. They found that the grouting and cementation process enhanced the deformation resistance of the rock and effectively prevented the gradual weakening and sliding of the fissures. Feng et al. (2021) studied the mechanical properties and failure modes of grouted coal rock mass specimens with bidirectional through fissures before and after grouting. They found that as the angle between the fissure direction and loading direction increased, the failure mode of the grouted specimens changed from compressive shear failure to sliding failure along the grout-rock interface, and eventually back to compressive shear failure. Sun et al. (2019) conducted rock mechanics tests on coal rock mass specimens with different grouting rates, revealing a significant linear relationship between the grouting rate and the peak strength and residual shear strength of the grouted specimens. Liu et al. (2018) grouted pre-cracked surrounding rock specimens and performed mechanical tests on the reinforced specimens. The results indicated that the peak strength, residual strength, internal structural integrity, rock stability, and deformation resistance of the grouted specimens significantly increased. Le et al. (2019) selected epoxy resin as the grouting material and conducted triaxial compression tests on rock-like specimens with different geometric shapes. The results showed that epoxy resin grouting could improve the peak strength of the specimens under triaxial compression.

From the above research, it can be seen that the physical and mechanical properties of grouting materials and the change law of mechanical properties of fractured rock mass before and after grouting reinforcement have been extensively studied, but mainly focused on the mechanical properties of precast fractured rock mass grouting reinforcement, while there are few related researches on broken rock mass before and after grouting reinforcement. This manuscript aims at the problem of roof surrounding rock deformation disease of small coal pillar gob-side entry in Maoduoshan Coal Mine, studies the mechanical behavior characteristics of four grouting material solidification samples in the process of uniaxial compression under different solidification time, on this basis, explores the strength recovery effect, crack propagation evolution and energy evolution law of complete surrounding rock samples and compressed broken samples before and after grouting reinforcement with four grouting materials, and puts forward the grouting reinforcement material suitable for the roof rock strata of small coal pillar gob-side entry. The research results can provide reference for grouting reinforcement design and deformation control of roadway surrounding rock. Future research can combine on-site monitoring data to validate the applicability of laboratory results and analyze the correlation between size effects and engineering conditions.

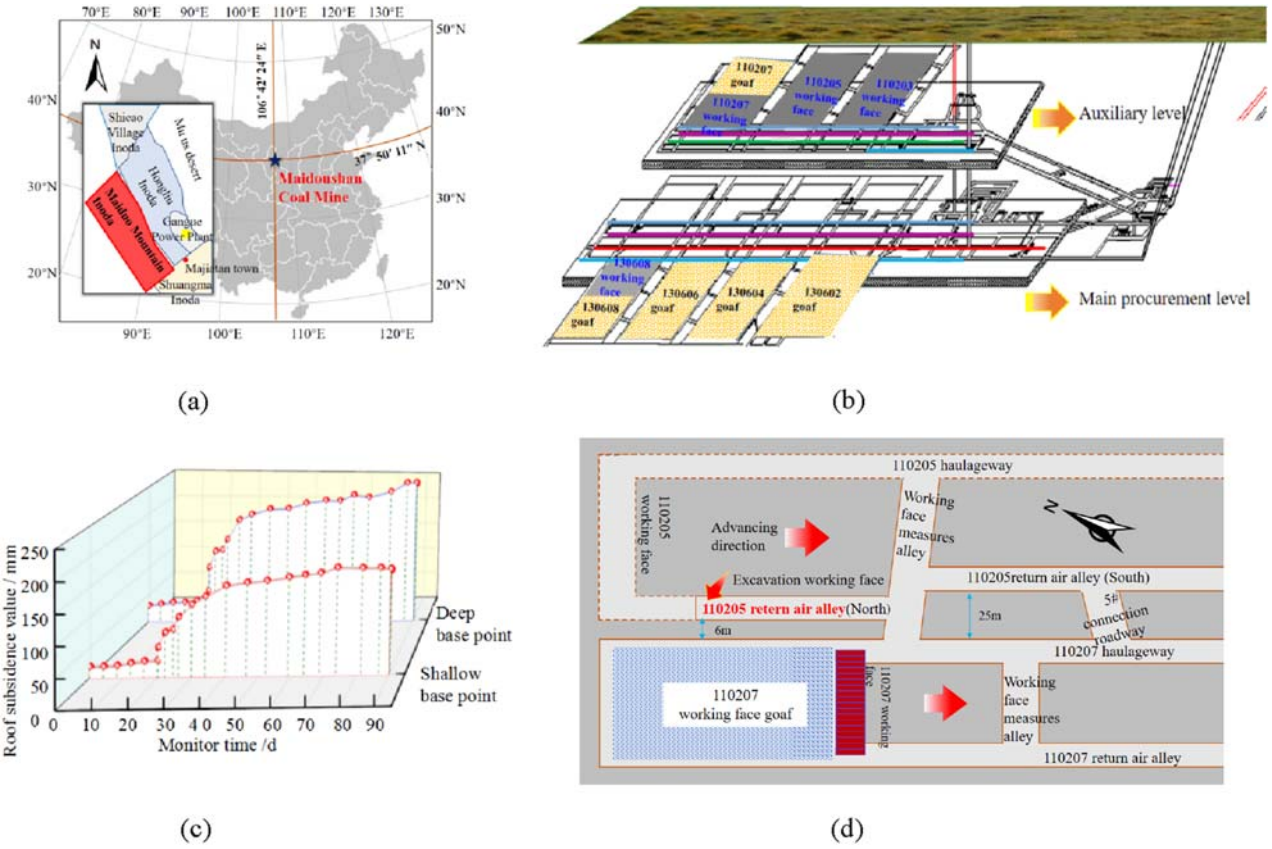

FIGURE 1
Engineering Background of Maidoushan Coal Mine. **(a)** Geographic location. **(b)** Stereoscopic schematic diagram. **(c)** Displacement variation curve of roadway surrounding rock roof. **(d)** 110205 working face return airway.

2 Experimental process

2.1 Engineering Background

Maidoushan Coal is located at the southern end of the Yuanyanghu mining area in Ningxia, with an area of 65 km2, reserves of 1.96 billion tons, and recoverable reserves of 1.13 billion tons (Figure 1a). The mine is divided into two zones and ten mining areas, with two production mining areas (13 and 11) and one preparation mining area (11N) (Figure 1b). The return airway roadway of the 110205 working face is located in the 11 mining area of the 2 # coal seam. The entire roadway is excavated along the roof of the 2 # coal seam, with the 110205 working face to the east, the 110207 working face machine roadway to the west, the 110205 working face airway to the south, and the 110205 working face measure roadway to the north (Figure 1d). The average burial depth is 309.4 m, the average coal thickness is 3.06 m, and the dip angle is 0°–7°. The direct top and bottom rock types are coarse and fine sandstone, with developed geological joints and poor integrity. By monitoring the deformation of the roof separation layer in the surrounding rock of the roadway, it was found that the subsidence values of the shallow and deep base points at a distance of 50 m from the excavation face were 151.20 mm and 209.31 mm, respectively, and continued to increase (Figure 1c). In response to this, cement grouting reinforcement measures were taken in severely deformed sections of the roadway, but the deformation was not completely controlled.

2.2 Sample preparation

To investigate the mechanical properties of grouting materials and clarify the recovery effect of bearing capacity of tunnel surrounding rock after grouting reinforcement, the entire experiment requires three types of samples, namely grouting material grouting consolidation sample, initial intact surrounding rock sample of roadway roof, and broken surrounding rock sample after grouting reinforcement.

Three types of ordinary cement, fly ash cement, and Portland cement originally used in coal mines, as well as one high-performance cement-based material, were selected as grouting materials. Mix four types of grouting materials with water and stir evenly. Load them into 70 mm × 70 mm × 70 mm cube molds and naturally solidify them indoors. The representativeness of sample size and on-site rock mass structure is preliminarily correlated through similarity ratio theory, and further verification through numerical simulation is required. After demolding, some standard cubic grouting material grouting consolidation samples of 70 mm

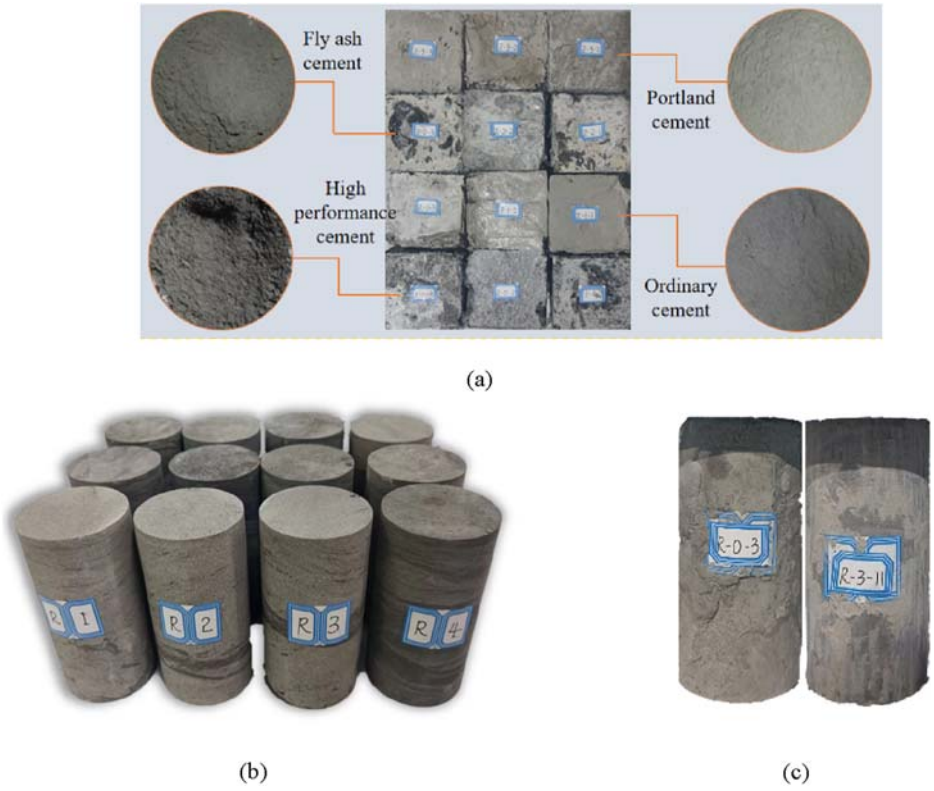

FIGURE 2
Samples required for the experiment. **(a)** Grouting materials and grouting grouting consolidation samples. **(b)** Initial intact surrounding rock samples. **(c)** Broken surrounding rock sample reinforced by grouting (Partial samples).

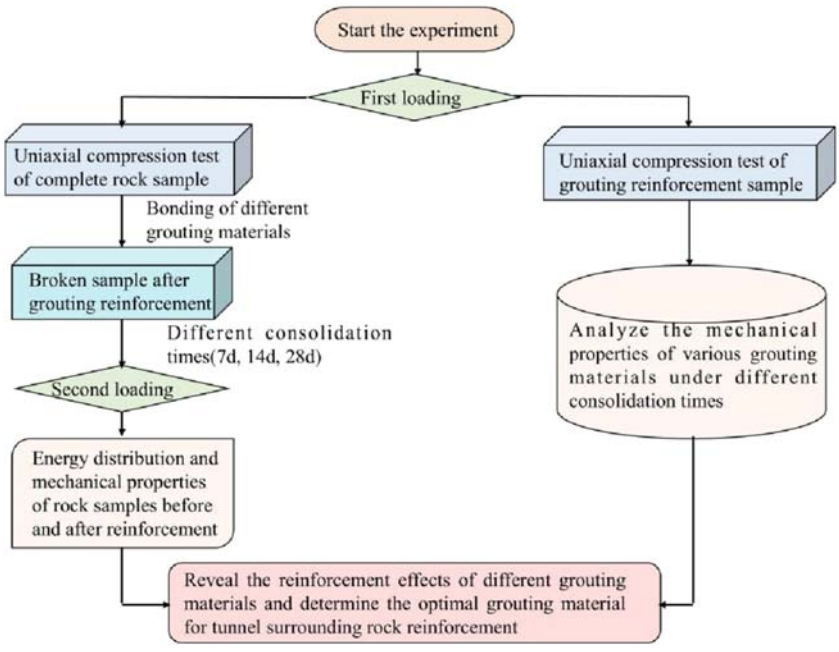

FIGURE 3
Schematic diagram of experimental method.

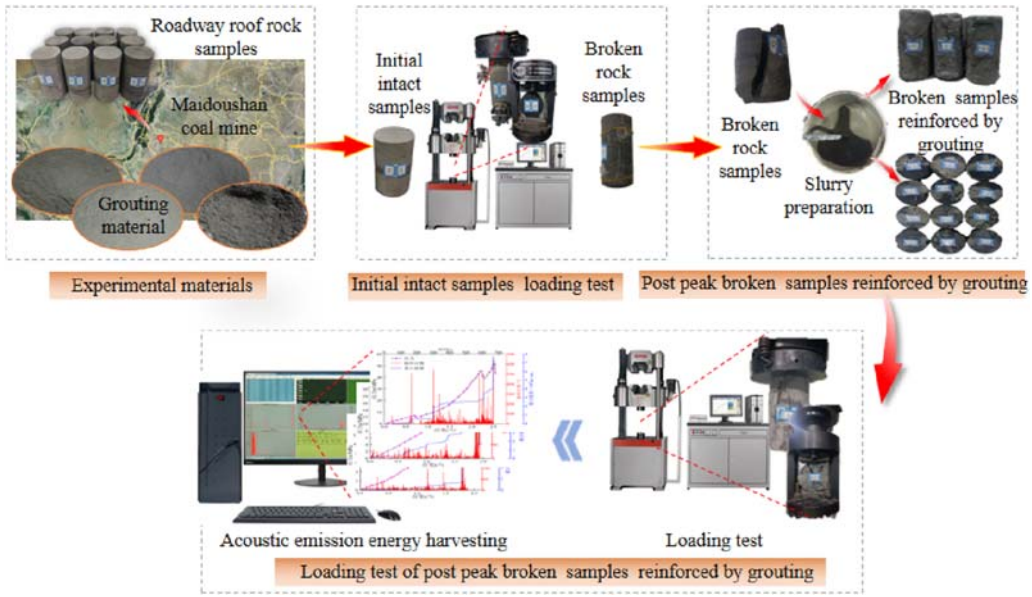

FIGURE 4
Experimental process of broken surrounding rock samples after grouting reinforcement.

× 70 mm × 70 mm were formed. Then, use a polishing machine to smooth the surfaces and reduce the influence of sample shape error on the test results (Figure 2a). To test the time effect of mechanical properties of each grouting material, three samples were made for each material, and indoor mechanical experiments were conducted after the samples were solidified under natural conditions for 7, 14, and 28 days, respectively.

The initial intact surrounding rock samples were transported to the laboratory for processing from the rock blocks at the top plate position of the roadway of the 110205 working face in Maidoushan Coal Mine. The sample is a cylindrical shape with a specification of Φ50 mm × 100 mm. The unevenness at both ends of the sample is ≤0.5 mm, the size error is ≤0.3 mm, and the error of the two end faces perpendicular to the axis is ≤0.5°, which meets the ISRM experimental standard of the International Committee on Rock Mechanics (Figure 2b).

The broken surrounding rock sample reinforced by grouting is mainly composed of crushed rock blocks compressed from the initial intact surrounding rock sample. After splicing them together according to the complete fracture surface, the existing four grouting materials are used to bond the rock mass into intact samples. The sample size remains a cylindrical body with dimensions of Φ 50 mm × 100 mm (Figure 2c). Considering the timeliness of the grouting material slurry, three samples were prepared for each grouting reinforcement, and then indoor mechanical experiments were conducted after 7, 14, and 28 days of consolidation under natural conditions to analyze the bonding effect of various grouting materials under different consolidation times. This provides a theoretical basis for the selection of grouting materials and grouting reinforcement parameters, as well as the design of reinforcement schemes in on-site engineering.

2.3 Experimental plan and equipment

The mechanical properties of the surrounding rock along the small coal pillar god-side entry and the degree of recovery of the bearing capacity of the surrounding rock after grouting reinforcement are the key factors in controlling the deformation of the roadway surrounding rock. According to the on-site geological data, the stress field of the surrounding rock of the 110205 small coal pillar god-side entry in Maidoushan Coal Mine shows a characteristic of horizontal stress being greater than vertical stress. During the excavation process of the working face, the surrounding rock stress of the roadway is redistributed, with horizontal stress transferring to the top and bottom plates and vertical stress transferring to both sides. As a result, there is a concentration of horizontal stress and a decrease in vertical stress at the top and bottom plate positions of the surrounding rock of the roadway. In view of this, the experimental plan in this article mainly includes uniaxial compression tests on consolidated specimens of grouting materials, intact surrounding rock samples, and uniaxial compression tests on broken surrounding rock samples after grouting reinforcement with grouting materials, as shown in Figure 3.

Uniaxial compression tests were conducted on grouting consolidation samples of different grouting materials, initial intact rock samples of surrounding rock roof, and broken surrounding rock samples after grouting reinforcement. The mechanical properties of each grouting material at different consolidation times and the strength recovery effect of post peak broken surrounding rock samples after grouting reinforcement were analyzed; The instrument used for uniaxial compression testing is the RMT-150B rock mechanics testing system, which can be equipped with

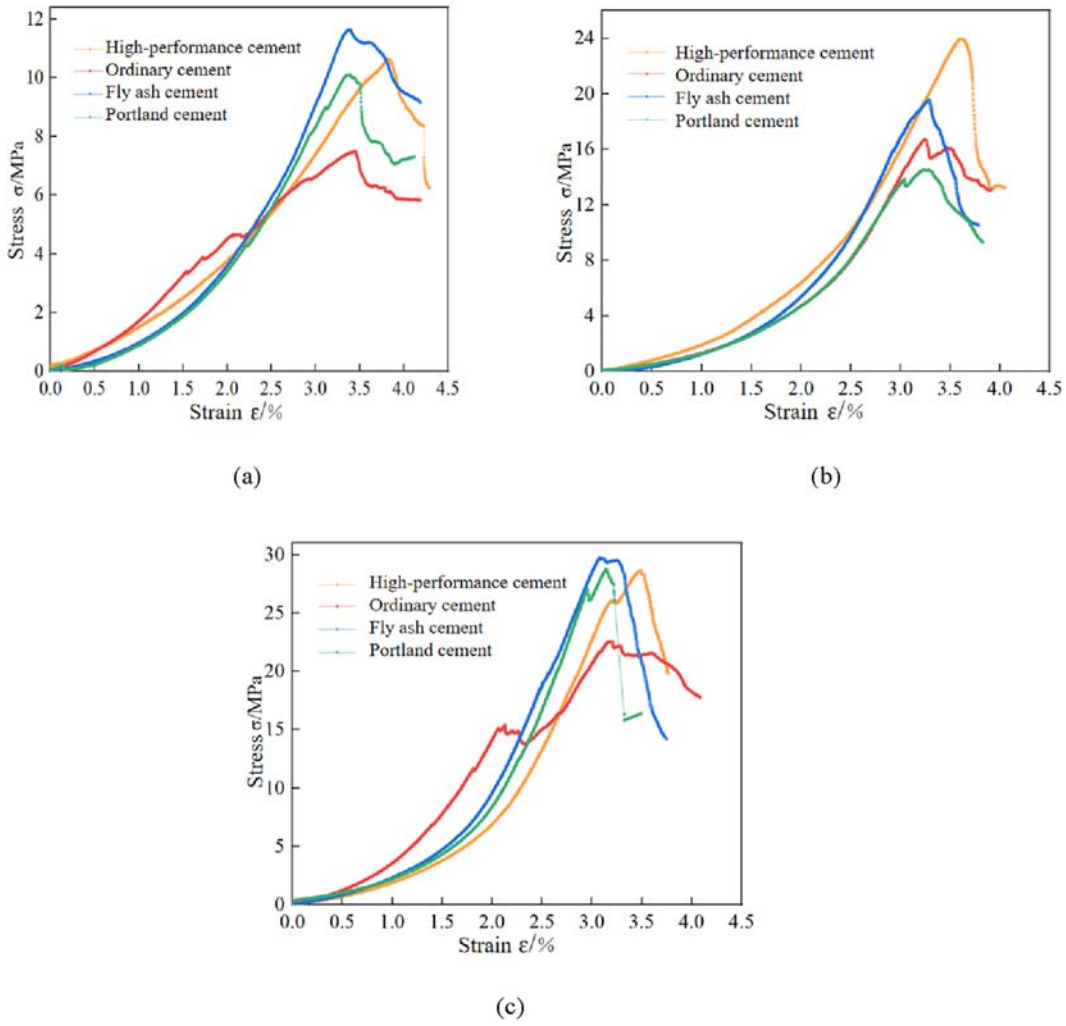

FIGURE 5
Strength curves of consolidated samples of various grouting materials at different consolidation times. **(a)** Consolidation time is 7 days. **(b)** Consolidation time is 14 days. **(c)** Consolidation time is 28 days.

a multi-channel acoustic emission (AE) synchronous monitoring system during the experimental process to monitor real-time indicators such as ringing count, amplitude, and energy during the damage evolution of samples. Four AE probes are arranged for each sample, and professional coupling agents are used to attach the probes to the side surface of the sample. By repeatedly adjusting the acoustic emission parameter values, the sampling frequency of the AE monitoring system for this experiment is determined to be a bandwidth of 1–400 kHz, a sampling rate of 3 MHz, a preamplifier gain value of 40 dB, To ensure data reliability, coupling agents are used in the test to ensure good sensor contact, and a 100 dB threshold is set to eliminate environmental background noise; Debug the sampling frequency and gain parameters multiple times to filter out signal artifacts (Figure 4).

3 Result analysis

3.1 Mechanical properties of grouting materials

3.1.1 Change characteristics of strength curves

The strength curves of consolidation specimens with different grouting materials after 7, 14, and 28 days of consolidation are shown in Figure 5.

From Figure 5, it can be seen that the uniaxial compressive strength of the consolidated specimens with different grouting materials ranges from 7.53 MPa to 12.00 MPa after 7 days of consolidation. Among them, the strength of the consolidated samples with fly ash cement grouting material and high-

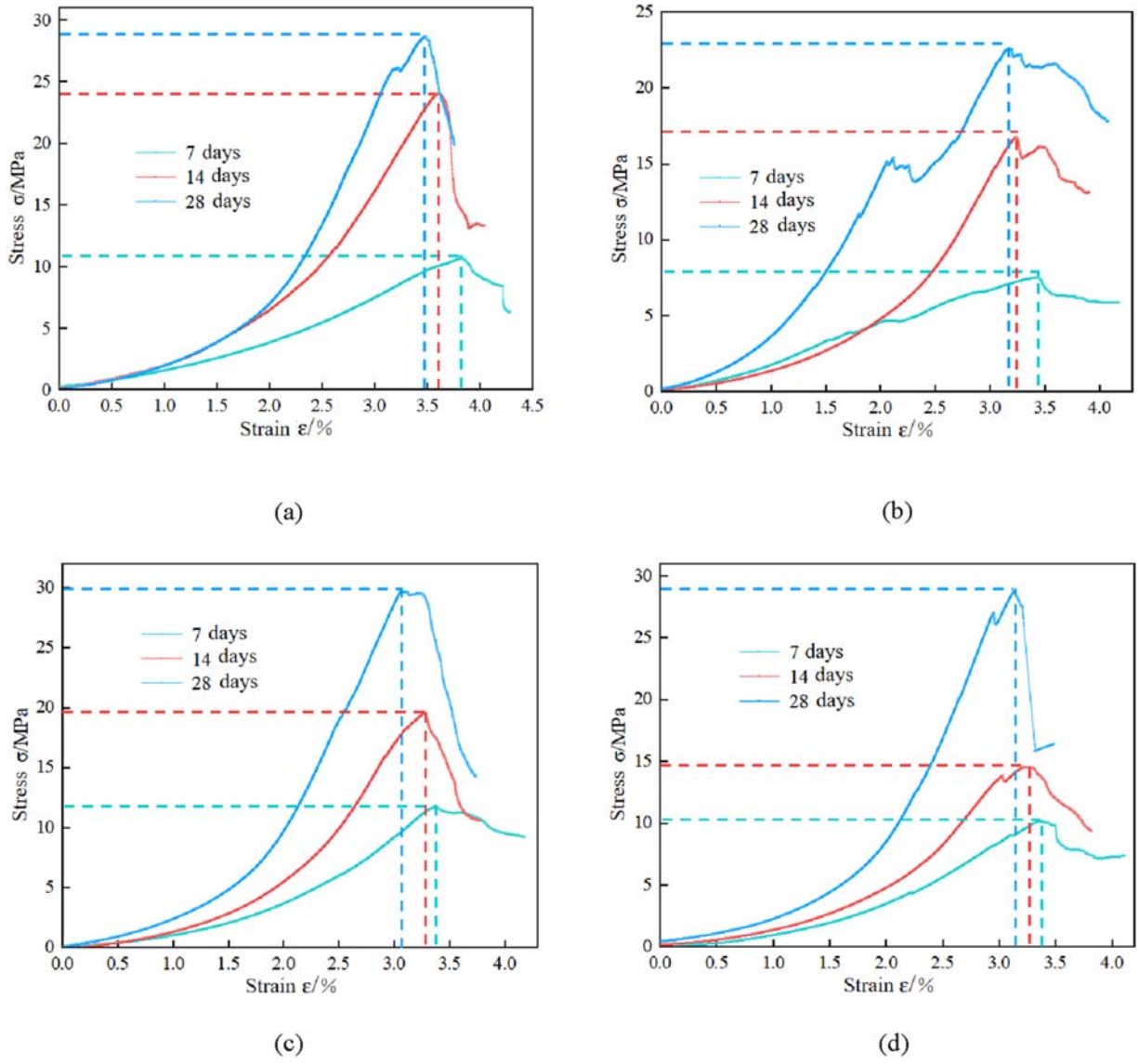

FIGURE 6
Relationship between strength curves and consolidation time of grouting consolidation samples of grouting materials. **(a)** High performance cement-based grouting material. **(b)** Ordinary cement grouting material. **(c)** Fly ash cement grouting material. **(d)** Portland cement grouting material.

performance cement-based grouting material is the highest, at 12.00 MPa and 11.20 MPa, respectively, followed by the consolidated samples with Portland cement grouting material and ordinary cement grouting material, with peak strengths of 10.04 MPa and 7.53 MPa, respectively; At 14 days of consolidation, the uniaxial compressive strength of each grouting material grouting consolidation sample ranged from 14.87 to 23.33 MPa. Among them, the recovery effect of the uniaxial compressive strength of the high-performance cement-based grouting material grouting consolidation sample was the most obvious, reaching 23.33 MPa. Then, the fly ash cement grouting material, ordinary cement grouting material, and silicate cement grouting material grouting consolidation samples, with corresponding strength values of 19.52 MPa, 16.88 MPa, and 14.87 MPa, respectively; At 28 days of consolidation, the uniaxial compressive strength of each grouting material grouting consolidation sample ranged from 23.07 MPa to 29.96 MPa. Among them, the strength of fly ash cement grouting material and high-performance cement-based grouting material grouting consolidation samples was the highest, at 29.96 MPa and 28.14 MPa, respectively. Then, the strength values of silicate cement grouting material and ordinary cement grouting material grouting consolidation samples were 28.03 MPa and 23.07 MPa, respectively.

Figure 5 illustrates that all grouting consolidation samples exhibit a pronounced initial compaction phase—attributable to inherent micro-defects—followed by an essentially linear elastic response, with only minor stress fluctuations observed in the ordinary cement specimens.

During the post-peak failure phase, all samples retain substantial residual strength and undergo significant plastic deformation, demonstrating notable ductility; notably, the fly ash cement and high-performance cement-based materials achieve the highest peak strengths, with the latter exhibiting a faster rate of strength gain.

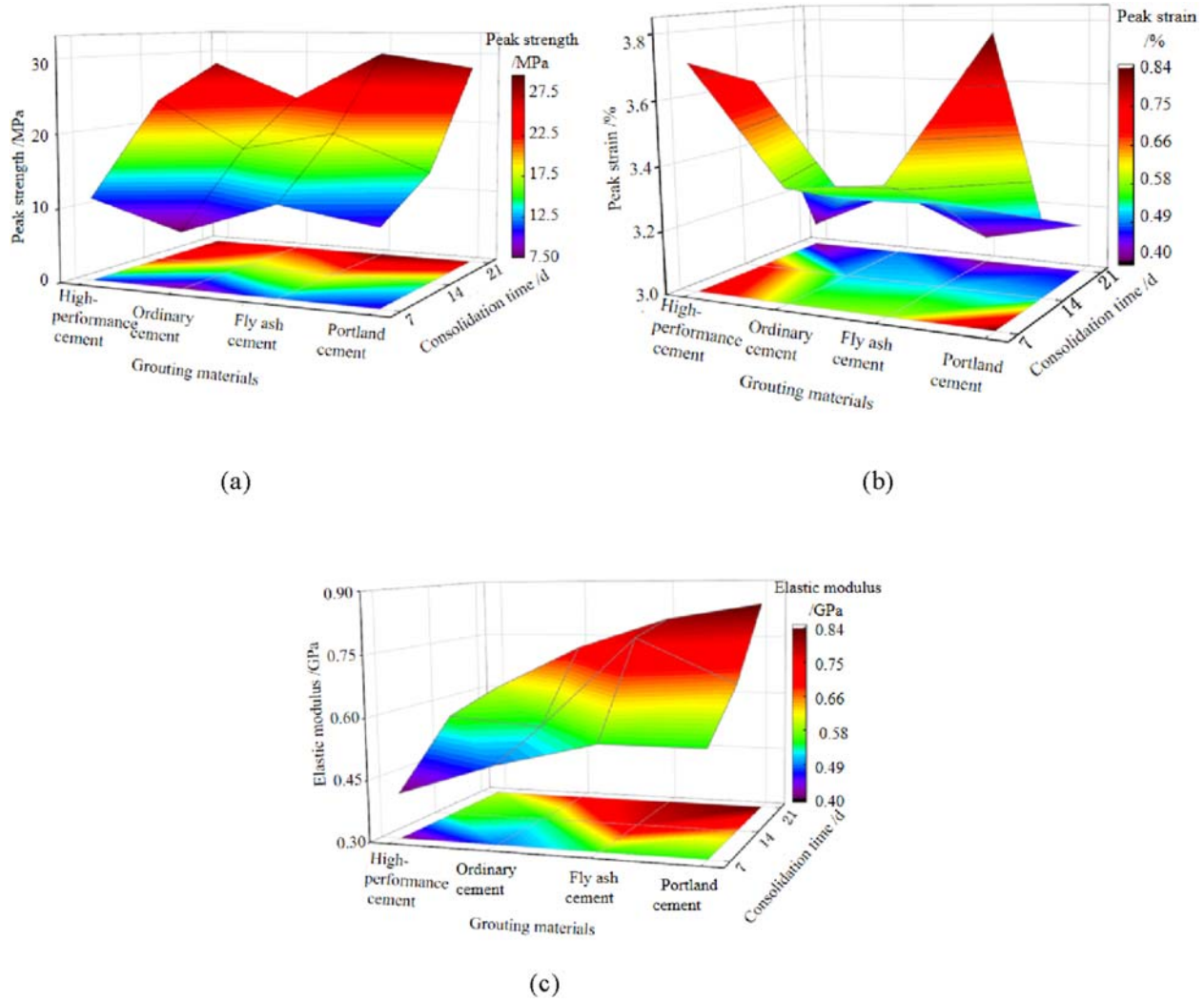

FIGURE 7
Variation characteristics of peak strength of grouting material grouting consolidation samples with grouting material and consolidation time. **(a)** Variation trend of peak strength with grouting material and consolidation time. **(b)** Variation trend of peak strain with grouting material and consolidation time. **(c)** Variation trend of elastic modulus with grouting material and consolidation time.

3.1.2 Time effect

The strength curves of each grouting material grouting consolidation samples under different consolidation times are shown in Figure 6.

As shown in Figure 6, with the increase of consolidation time, the peak strength of each grouting material grouting consolidation sample continues to increase, but the peak strain decreases, indicating that the bearing capacity of different grouting materials grouting consolidation samples increases continuously during the consolidation process, while their ductility transitions towards brittleness. Comparative analysis of stress-strain curves shows that the recovery of bearing capacity of different grouting materials is related to the consolidation time. Among them, the strength recovery effect of high-performance cement-based grouting material and ordinary cement grouting material is significant at 14 days of consolidation, while the strength recovery effect of fly ash cement grouting material and silicate cement grouting material is relatively small at 14 days and 14–28 days of consolidation. This indicates that the use of high-performance cement-based grouting material and ordinary cement grouting material in engineering can achieve self strength recovery in a shorter time.

3.1.3 Change law of strength parameters

The peak strength, peak strain, and elastic modulus of each grouting material grouting consolidation sample under different consolidation times can be used as important indicators to evaluate its mechanical properties. Draw a graph showing the relationship between the peak strength, peak strain, and elastic modulus of each grouting material grouting consolidation sample under compression with the type of grouting material and consolidation time. Analyze the mechanical properties of each grouting material, and establish the suitable grouting material for the small coal pillar god-side entry roadway in Maidoushan Coal Mine. The relationship between the peak strength, peak strain, and elastic modulus of the grouting

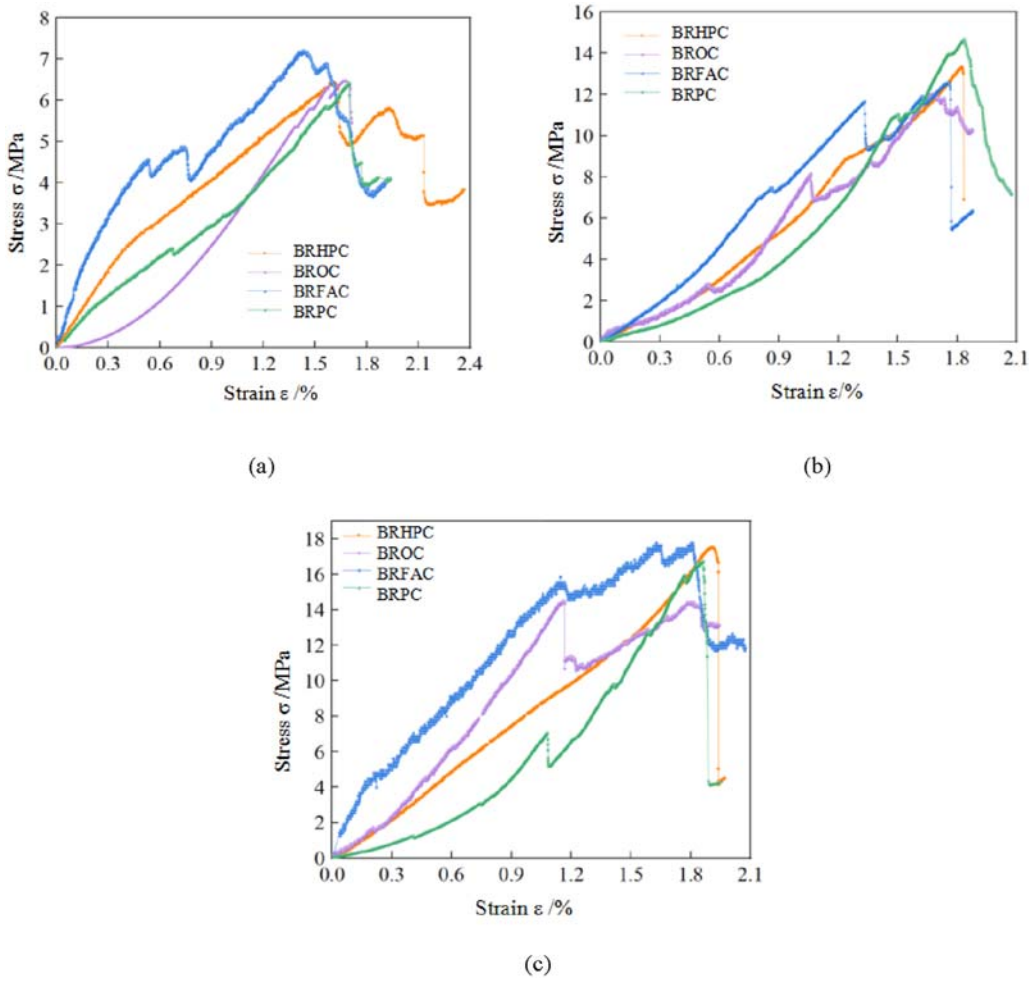

FIGURE 8
Stress strain curves of broken surrounding rock samples reinforced by grouting materials under different consolidation times. **(a)** The consolidation time is 7 days. **(b)** The consolidation time is 14 days. **(c)** The consolidation time is 28 days. Note: BRHPC-Broken rock sample reinforced with high-performance cement; BROC-Broken rock sample reinforced with ordinary cement; BRFAC-Broken rock sample reinforced with fly ash cement; BRPC-Broken rock sample reinforced with portland cement.

material grouting consolidation samples and the type of grouting material and consolidation time is shown in Figure 7.

Figure 7a shows that the peak strength of the consolidated samples of the four grouting materials increases significantly with the increase of consolidation time. Among them, the peak strength of high-performance cement-based grouting material and fly ash cement grouting material is at its highest at any consolidation time, while the peak strength of ordinary cement grouting material and Portland cement grouting material is not significantly different. The peak strengths of high-performance cement-based grouting material and fly ash cement grouting material were 23.33 MPa and 19.52 MPa respectively after 14 days of consolidation, and 28.14 MPa and 29.96 MPa respectively after 28 days of consolidation, indicating that the strength recovery rate of high-performance cement-based grouting material is relatively fast.

From Figure 7b, it can be seen that the peak strain of the consolidated samples of the four grouting materials decreases continuously with the increase of reinforcement time, indicating a transition from ductility to brittleness of the grouting materials. Comparing the peak strain difference between 28 days and 7 days of consolidation for each grouting material, the peak strain difference between Portland cement grouting material and fly ash cement grouting material was the highest, at 0.66 and 0.30, respectively. However, the peak strain difference between high-performance cement-based grouting material and ordinary cement grouting material was lower, at 0.24 and 0.14, respectively. This indicates that high-performance cement-based grouting material and ordinary cement grouting material can more effectively exert consolidation effect in the reinforcement process, which is beneficial for practical engineering practice.

As shown in Figure 7c, with the increase of reinforcement time, the elastic modulus of the consolidated samples of the four grouting materials increases. At any given consolidation time, the elastic modulus growth rate of high-performance cement-based grout is the smallest, indicating that the rigidity of high-performance cement-based grout is relatively low and it has good ductility.

Due to the grouting reinforcement of the surrounding rock of the roadway, good timeliness is required for controlling the

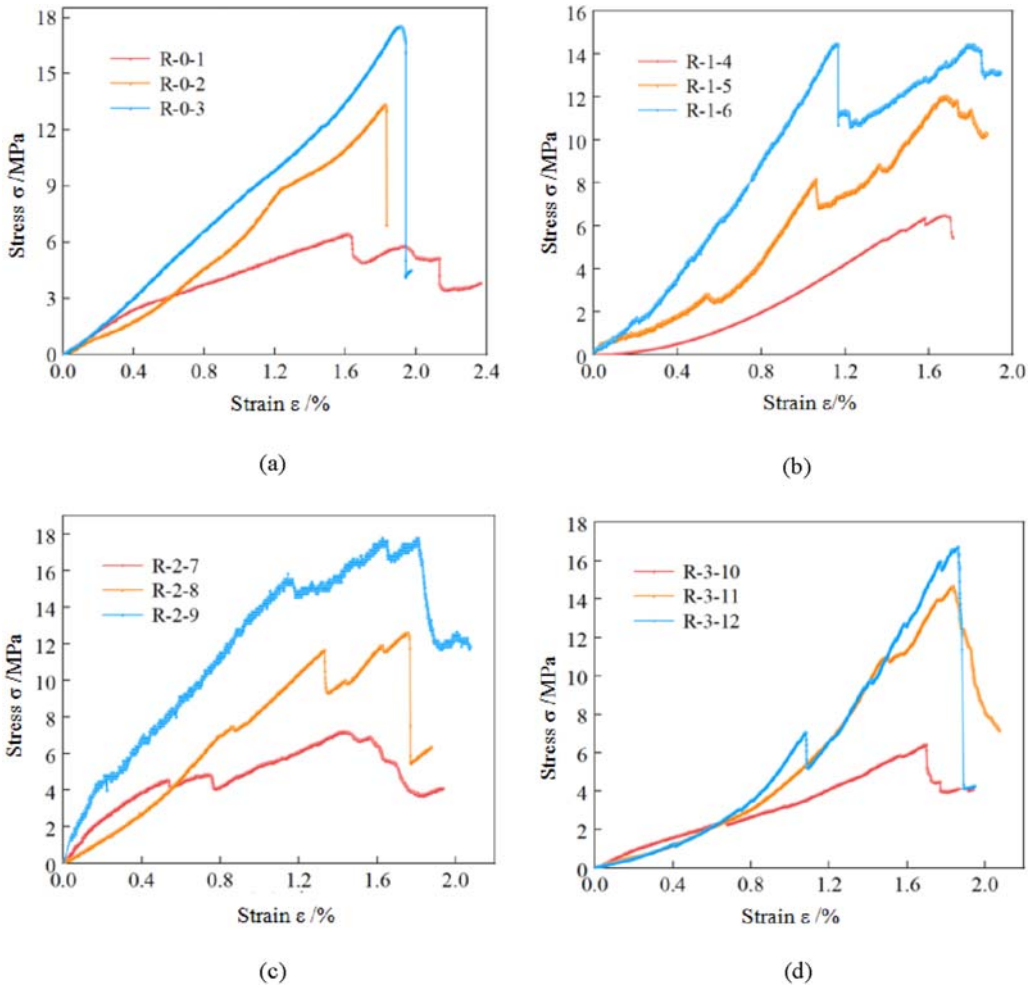

FIGURE 9
Change characteristics of strength curves of broken surrounding rock samples reinforced by different grouting with consolidation time. **(a)** High performance cement-based grouting material. **(b)** Ordinary cement grouting material. **(c)** Fly ash cement grouting material. **(d)** Portland cement grouting material.

surrounding rock deformation. The shorter the control time, the better the reinforcement effect. Compared with other reinforcement methods such as anchor support and grouting anchor coordination, high-performance cement-based materials have more advantages in short-term strength recovery, At the same time, the higher the self bearing strength, ductility, and buffering performance of the grouting material, the better the safety guarantee for the efficient production of coal resources in the mine. Therefore, high-performance cement-based grouting slurry has great practical value for on-site engineering.

3.2 Grouting reinforcement effect of broken surrounding rock samples

Rock mechanics experiments are an effective means of reflecting the mechanical properties of surrounding rock in engineering sites. The rock samples obtained on site are compressed to form broken surrounding rock samples, and then different grouting materials are used to paste the broken surrounding rock samples to form grouting reinforcement samples. Finally, compression tests are conducted on the broken surrounding rock samples reinforced with different grouting materials to analyze the mechanical behavior characteristics of the reinforced broken surrounding rock samples and obtain the optimal grouting reinforcement materials, providing reference for engineering practice.

3.2.1 Change characteristics of strength curves

Different grouting materials were used to reinforce the broken surrounding rock samples. The reinforced samples were subjected to uniaxial compression tests after consolidation for 7, 14, and 28 days. The strength curves of the broken surrounding rock samples after grouting reinforcement with different grouting materials are shown in Figure 8.

Figure 8a indicates that, after 7 days of consolidation, the uniaxial compressive strengths of grouted broken rock samples span 6.8–7.8 MPa with minimal variation in peak strain, confirming their basic load-bearing capacity and similar early reinforcement

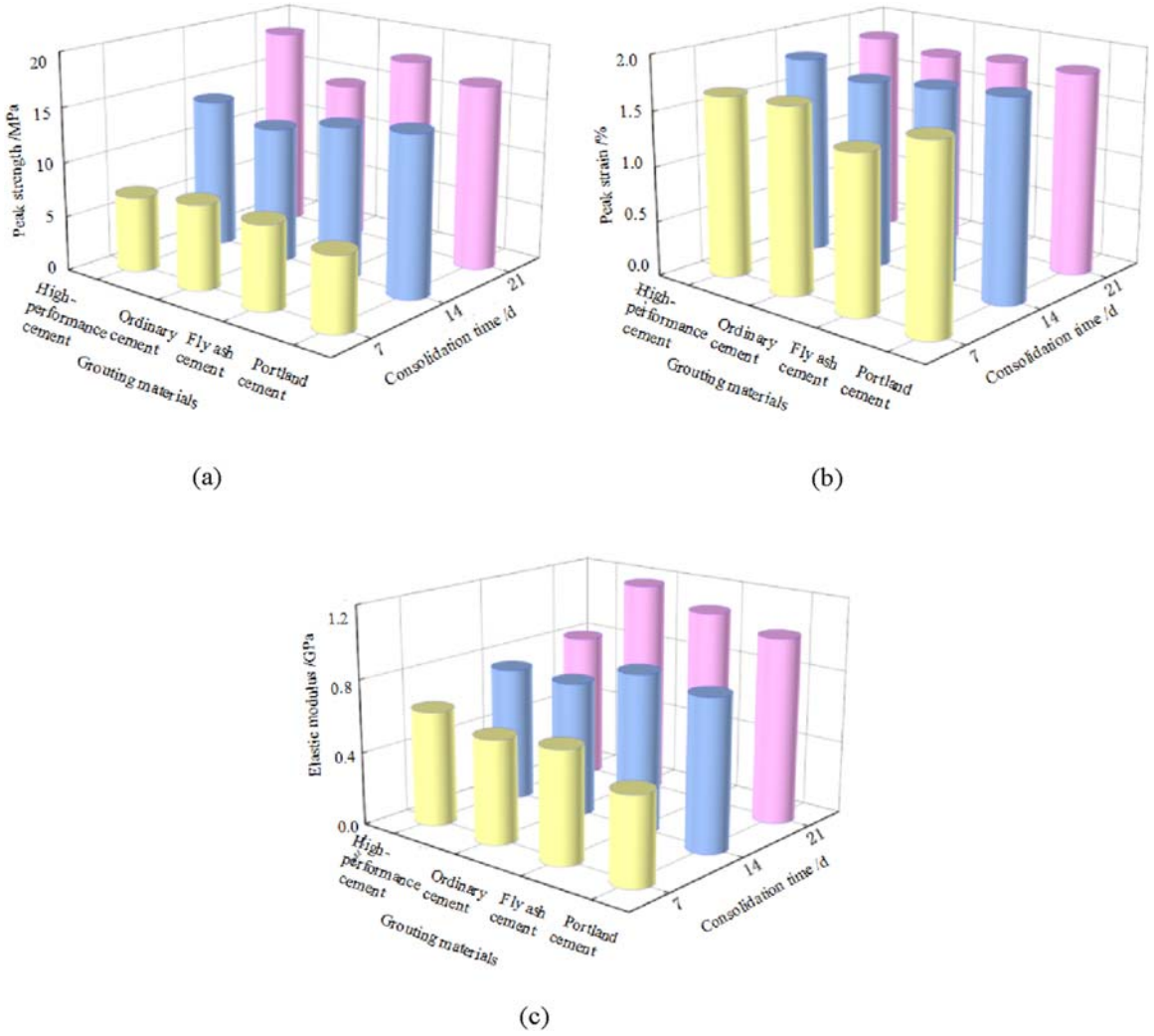

FIGURE 10
Variation characteristics of mechanical parameters of broken surrounding rock samples reinforced by grouting with grouting materials and consolidation time. **(a)** Variation trend of peak strength with grouting material and consolidation time. **(b)** Variation trend of peak strain with grouting material and consolidation time. **(c)** Variation trend of elastic modulus with grouting material and consolidation time.

effects. Moreover, during the compaction phase, fly ash cement, high-performance cement-based, and Portland cement specimens display convex stress–strain profiles, whereas ordinary cement specimens exhibit a concave trend, reflecting material-dependent microstructural alterations induced by grouting. In the post-peak phase, all reinforced samples maintain substantial residual strength and exhibit pronounced plastic deformation, evidencing significant ductility shortly after grouting; notably, the high-performance cement-based specimens outperform other materials in post-peak toughness.

From Figure 8b, it can be seen that the uniaxial compressive strength of the broken surrounding rock samples reinforced with different grouting materials after 14 days of consolidation ranges from 12.4 MPa to 14.7 MPa. Compared with the strength of the samples after 7 days of consolidation, the uniaxial compressive strength of the samples significantly increases, indicating that the reinforcement effect of grouting materials has a significant time effect. According to Figure 8c, at 28 days of consolidation, the uniaxial compressive strength of the broken surrounding rock samples reinforced with different grouting materials ranged from 14.6 MPa to 18.6 MPa. Compared with the samples at 14 days of consolidation, the uniaxial compressive strength further increased, but the growth was slow, indicating that the strength recovery of the broken surrounding rock samples reinforced with grouting was more significant in the early stage of consolidation.

The strength curves of broken surrounding rock samples reinforced by grouting with various grouting materials at different consolidation times are shown in Figure 9. As shown in the figure, the strength curve of the broken surrounding rock reinforced by high-performance cement-based grouting material shows a relatively stable trend at 7, 14, and 28 days of consolidation. In the pre peak stage, the strength curve increases in a nearly linear form, showing strong elastic characteristics. However, the strength curves of the broken surrounding rock samples reinforced by ordinary

TABLE 1 Preparation plan for experimental rock samples.

Sample number	Initial intact surrounding rock samples	Broken surrounding rock samples	Consolidation time/d	Grouting material
ZJL-0–1	R1	R-0–1	7	High performance cement
ZJL-0–2	R2	R-0–2	14	
ZJL-0–3	R3	R-0–3	28	
ZJL-1–1	R4	R-1–4	7	Ordinary cement
ZJL-1–2	R5	R-1–5	14	
ZJL-1–3	R6	R-1–6	28	
ZJL-2–1	R7	R-2–7	7	Fly ash cement
ZJL-2–2	R8	R-2–8	14	
ZJL-2–3	R9	R-2–9	28	
ZJL-3–1	R10	R-3–10	7	Portland cement
ZJL-3–2	R11	R-3–11	14	
ZJL-3–3	R12	R-3–12	28	

TABLE 2 Strength recovery degree of broken surrounding rock samples after grouting reinforcement.

Grouting materials	High performance cement			Ordinary cement			Fly ash cement			Portland cement		
Consolidation time/d	7	14	28	7	14	28	7	14	28	7	14	28
Strength of intact surrounding rock samples/MPa	50.8	51.4	51.7	52.1	51.8	57.9	57.4	58.2	54.4	60.0	50.8	50.5
Strength of broken surrounding rock samples reinforced by grouting/MPa	6.9	13.7	18.6	7.8	12.4	14.6	7.7	13.9	18.0	6.8	14.7	16.9
Strength recovery degree/%	13.6	26.7	36.0	15.0	23.9	25.2	13.4	23.9	33.1	11.3	28.9	33.5

cement grouting material and silicate cement grouting material show a concave growth trend, and there are fluctuations during the growth process. The strength curve of the broken surrounding rock sample reinforced with fly ash cement grouting material shows an upward convex growth trend, accompanied by fluctuating pressure relief phenomenon. It can be seen that high-performance cement-based grouting materials have good grouting reinforcement effects.

3.2.2 Change law of strength parameters

The peak strength, peak strain and elastic modulus of each grouting material grouting reinforcement broken surrounding rock samples under different consolidation time can be used as an important index to evaluate the reinforcement effect of grouting material. The variation characteristics of mechanical parameters of broken surrounding rock samples reinforced by grouting with grouting materials and consolidation time is shown in Figure 10.

Figure 10a shows that the peak strength of the surrounding rock samples reinforced with four types of grouting materials shows a significant increasing trend with the increase of consolidation time. Among them, the peak strength of the broken surrounding rock samples reinforced with high-performance cement-based grouting materials and fly ash cement grouting materials is at its highest at any consolidation time, while the peak strength of the broken surrounding rock samples reinforced with ordinary cement grouting materials is the lowest. From this, it can be seen that high-performance cement-based grouting materials and fly ash cement grouting materials have better reinforcement effects on broken surrounding rock samples than other grouting materials.

As shown in Figure 10b, with the increase of consolidation time, the peak strain of the broken surrounding rock samples reinforced by various grouting materials increases continuously. At 28 days of consolidation, the peak strain of the broken surrounding rock samples reinforced with various grouting materials ranged from 1.77% to 1.84%. Among them, the peak strain of the broken surrounding rock samples reinforced with

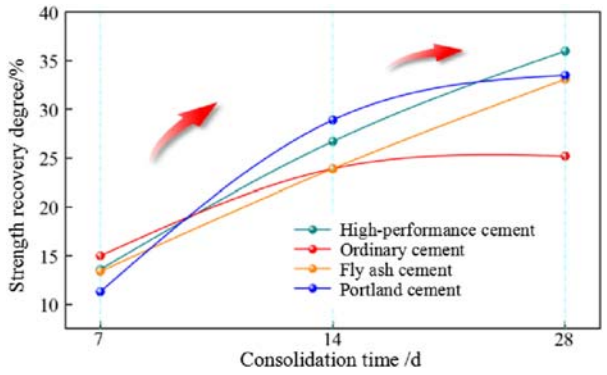

FIGURE 11
Strength recovery degree of broken surrounding rock samples reinforced by different grouting materials.

high-performance cement-based grouting materials was the highest, indicating that high-performance cement-based grouting materials can fully exert their own deformation during the grouting reinforcement process and achieve the function of buffering disturbance loads.

Figure 10c shows that as the consolidation time increases, the elastic modulus of the broken surrounding rock samples reinforced by various grouting materials increases. At 7 days and 14 days of consolidation, the elastic moduli of the broken surrounding rock samples reinforced with various grouting materials were found to be between 0.48-0.63 GPa and 0.81–1.18 GPa, respectively. Among them, the elastic modulus of the broken surrounding rock samples reinforced with high-performance cement-based grouting materials increased at the smallest rate with consolidation time. It can be seen that the stiffness of the broken surrounding rock sample reinforced by high-performance cement-based grout injection is relatively small, and it can produce significant elastic deformation under the same stress, which helps to buffer the severe damage caused by short-term disturbance loads.

3.2.3 Strength recovery effect

The strength curves of the initial intact surrounding rock sample and the broken surrounding rock sample after the grouting reinforcement peak were analyzed to explore the reinforcement effect of each grouting material on the strength recovery of the broken surrounding rock sample. In order to quantitatively reflect the strength recovery effect of broken surrounding rock samples, the ratio between the strength of broken surrounding rock sample after grouting reinforcement and the strength of initial intact surrounding rock sample is used in this manuscript as an important index to evaluate the grouting reinforcement effect. The strength recovery degree of broken surrounding rock samples reinforced by different grouting is shown in Table 2 and Figure 11.

It can be seen from Table 2 and Figure 11 that within the consolidation time of 7–28 days, the strength recovery degree of each grouting reinforcement broken surrounding rock sample shows different growth trends with the increase of consolidation time. The strength recovery degree of the samples reinforced with ordinary cement grouting material and Portland cement grouting material shows an upward convex increasing trend with the consolidation time; The strength recovery degree of the samples reinforced with high-performance cement-based grouting material and fly ash cement grouting material showed a linear function growth trend with the consolidation time, and the strength recovery degree of the samples reinforced with high-performance cement-based grouting material was higher than that of the samples reinforced with fly ash cement grouting material. When the consolidation time is 28 days, the strength recovery values of broken surrounding rock samples reinforced by high-performance cement-based grouting materials, Portland cement grouting materials, fly ash cement grouting materials and ordinary cement grouting materials are 36.0%, 33.5%, 33.1% and 25.2% respectively, and the influence of high-performance cement-based grouting materials and fly ash cement grouting materials on the strength recovery of broken surrounding rock samples is still growing steadily after 28 days.

3.2.4 Damage evolution characteristics

Through the above analysis of the mechanical properties of four different grouting reinforcement samples and the strength recovery degree of grouting reinforcement broken surrounding rock samples, it can be seen that the mechanical properties of high-performance cement-based grouting material grouting reinforcement broken surrounding rock samples are significantly better than those of other three grouting materials grouting reinforcement broken surrounding rock samples. Therefore, taking the loading process of broken surrounding rock samples reinforced by high-performance cement-based grouting under different consolidation time as an example, the strength recovery effect of broken surrounding rock samples are analyzed. During the AE process, the ringing count reflects the frequency of microcrack activity, which usually increases rapidly during the stress peak stage before sample failure; The accumulated energy represents the total energy released by crack propagation, which can characterize the overall strength of failure and the severity of the failure process. The curves of stress, strain, ring count, and cumulative energy versus consolidation time of the initial intact surrounding rock sample and the grouting reinforced broken surrounding rock sample during loading are shown in Figure 12.

A large number of practice shows that the consolidation time of grouting material slurry plays a great role in controlling the deformation of broken surrounding rock. At the 7th day of consolidation, the maximum ring count and the total cumulative energy of the initial intact surrounding rock sample are 850 and 6.5×10^5mvms, respectively, and the ring count is mainly displayed in the sample broken stage, while the ring count in other stages is relatively small. During the whole loading process, the broken surrounding rock sample reinforced by grouting has been producing acoustic emission signals. The maximum number of cycles and cumulative energy of the entire process are 240 and $2.7 \times {}^{104\text{mv}}$ms, respectively, which are much smaller than the maximum number of cycles and cumulative energy of the initial intact rock sample. Moreover, the cumulative energy of acoustic emission is positively correlated with the rock damage variable D, which is consistent with the Lemaitre strain equivalence hypothesis. The results indicate that the grouting material has a relatively small bonding effect on the reinforcement of fractured rock samples on the 7th day of consolidation, and

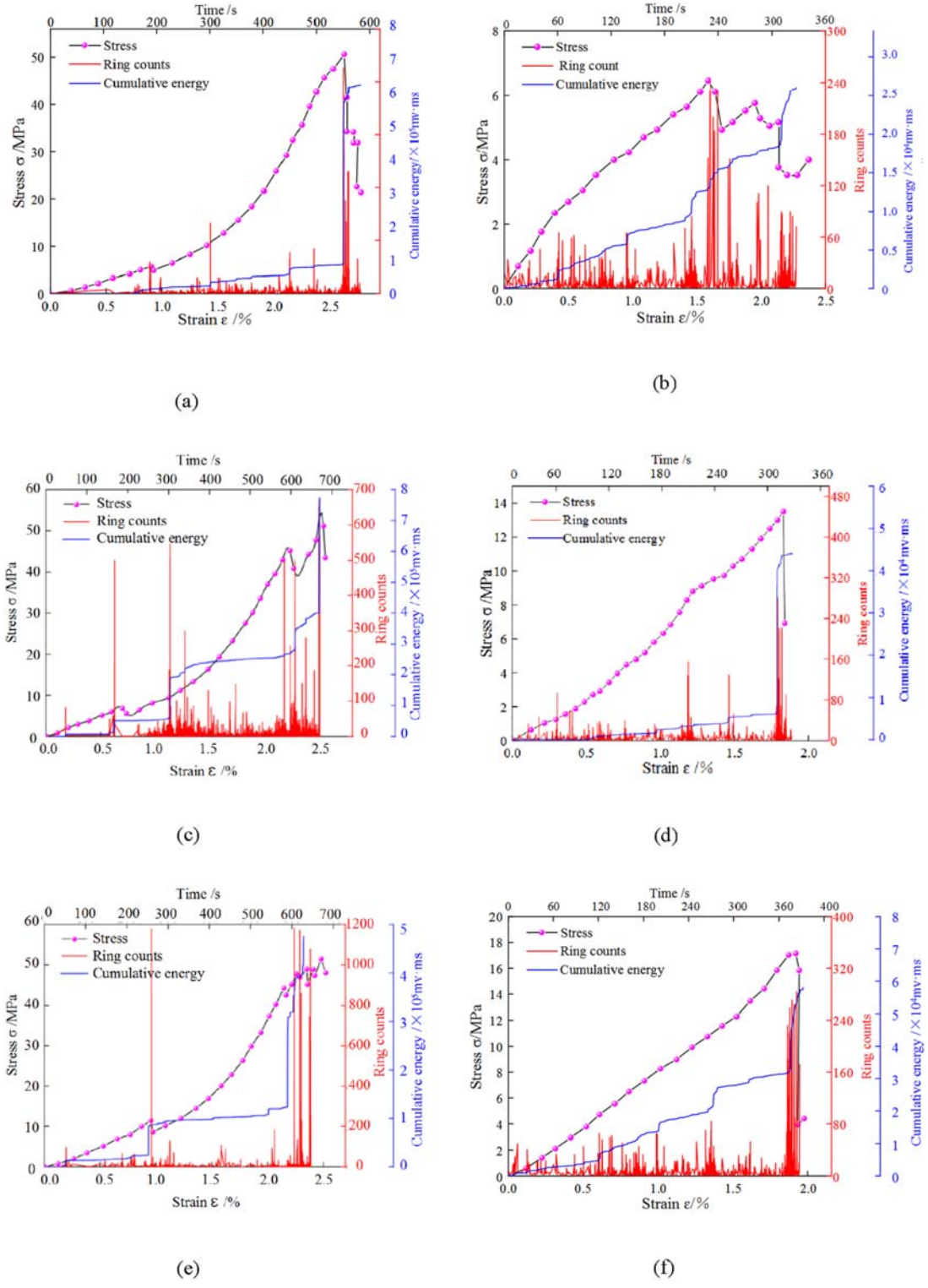

FIGURE 12
AE damage evolution curves of broken surrounding rock samples reinforced by grouting. **(a)** The initial intact surrounding rock sample R1. **(b)** Broken confining pressure rock sample R-0–1 consolidated for 7 days. **(c)** The initial intact surrounding rock sample R2. **(d)** Broken confining pressure rock sample R-0–2 consolidated for 14 days. **(e)** The initial intact surrounding rock sample R3. **(f)** Broken confining pressure rock sample R-0–3 consolidated for 28 days.

the grouting material achieves damage repair by suppressing crack propagation.

At the 14th and 28th day of consolidation, the maximum ring count of the initial intact surrounding rock samples exceeded 1,000 and 1,200 respectively, and the cumulative energy reached 7.8 $\times$ 10^5mvms and 4.5 $\times$ 10^5mvms, respectively. During the whole loading process, the broken surrounding rock sample reinforced by grouting has been producing acoustic emission signals, and the ring count in the broken stage is about 300, which is less than the maximum value of the ring count of the initial complete surrounding rock sample. The cumulative energy of the broken surrounding rock sample reinforced by grouting in the whole process is 4.7 $\times$ 10^4mvms and 6.0 $\times$ 10^4mvms, respectively, which is one order of magnitude less than the relevant parameters of the complete surrounding rock sample. It shows that the reinforcement effect of grouting material is significant at the 14th day after grouting reinforcement of broken surrounding rock sample.

From the above acoustic emission damage evolution characteristics of surrounding rock samples, it can be seen that the evolution forms of stress, strain, crushing time, ringing count and accumulated energy of the initial intact surrounding rock samples have the same regularity. The energy event mainly occurs in the stress peak stage, and the acoustic emission signals generated in other stages are less. Compared with the intact surrounding rock sample, the stress, strain, ringing count and cumulative energy of the grouting reinforced broken surrounding rock sample are significantly reduced, and show a significant linear positive correlation with the consolidation time, indicating that the strength recovery effect of the grouting reinforced broken surrounding rock sample is closely related to the consolidation time.

4 Conclusion

Aiming at the large deformation problem of surrounding rock of small coal pillar gob side entry in Maiduoshan coal mine, with the help of rock mechanics test loading system and acoustic emission synchronous monitoring system, the mechanical behavior characteristics of four kinds of grouting material samples and four kinds of grouting material grouting reinforcement surrounding rock samples were studied, the strength recovery effect of broken rock samples after grouting reinforcement was revealed, and the optimal grouting reinforcement material was obtained. The main conclusions are as follows:

(1) A comprehensive comparison of the mechanical properties of the four grouting materials shows that the consolidation time of high-performance cement-based grouting materials is the shortest, which can rapidly improve the strength of broken rock samples, and has great application value in engineering practice. The correlation between the microstructure and macroscopic mechanical behavior of different materials needs further research to reveal the multi-scale strengthening mechanism

(2) Compared with the strength curves of broken surrounding rock samples reinforced by Portland cement grouting materials, fly ash cement grouting materials and ordinary cement grouting materials, the strength curves of broken surrounding rock samples reinforced by high-performance cement-based grouting materials showed a steady growth trend, without obvious pressure relief and fluctuation, indicating that the strength recovery effect of broken surrounding rock samples reinforced by high-performance cement-based grouting materials was relatively stable.

(3) In this paper, the strength recovery effect of broken specimens after grouting reinforcement is defined. When the consolidation time is 28 days, the strength recovery degree of the four grouting materials after grouting reinforcement is in the order of high-performance cement-based grouting material, Portland cement grouting material, fly ash cement grouting material and ordinary cement grouting material, and the strength recovery values are 36.0%, 33.5%, 33.1% and 25.2% respectively. At the same time, the strength of the samples reinforced by high-performance cement-based grouting material and fly ash cement grouting material still has a stable growth. Subsequent on-site tests are required to verify the material properties, optimize reinforcement schemes under different geostress conditions based on cost-benefit analysis, suggest selecting a test section at the 110205 working face of the coal mineand monitor the deformation of surrounding rock and acoustic emission signals after grouting to quantify the on-site application effect.

(4) During the loading process of the initial intact surrounding rock sample, the energy event mainly occurred in the stress peak, and the acoustic emission signals produced in the other stages were less. Compared with the initial intact surrounding rock sample, the stress, strain, ring count and cumulative energy of the grouting reinforced broken surrounding rock sample are significantly reduced, and show a significant linear positive correlation with the consolidation time. Considering that the reinforcement effect increases with the curing time, it is recommended to further optimize the on-site reinforcement time strategy based on construction progress and safety requirements, in order to achieve a dual improvement in reinforcement efficiency and mechanical performance.

Data availability statement

The raw data supporting the conclusions of this article will be made available by the authors, without undue reservation.

Author contributions

ZS: Writing – original draft, Project administration, Conceptualization, Methodology, Writing – review and editing. SY: Data curation, Writing – original draft, Software, Investigation. CJ: Formal Analysis, Writing – original draft, Funding acquisition. LX: Supervision, Writing – review and editing, Resources. WL: Validation, Writing – review and editing, Visualization.

Funding

The author(s) declare that financial support was received for the research and/or publication of this article. This study was funded by the National Natural Science Foundation of China (Grant No. 52274138) and the Shaanxi Province postdoctoral research project (Grant No. 2023BSHEDZZ313). Their support is gratefully acknowledged.

Conflict of interest

The authors declare that the research was conducted in the absence of any commercial or financial relationships that could be construed as a potential conflict of interest.

Generative AI statement

The author(s) declare that no Generative AI was used in the creation of this manuscript.

Publisher's note

References

Cao, F. Z., and Yan, P. Y. (2019). The influence of the hydration procedure of mgo expansive agent on the expansive behavior of shrinkage-compensating mortar. *Constr. Build. Mater.* 202, 162–168. doi:10.1016/j.conbuildmat.2019.01.016

Feng, H., Zhang, X. M., Zhou, X. S., Zhang, C., and Chen, X. (2021). Experimental study on the compression behavior of grouted rock with bi-directional penetrating crack. *Appl. sciences-basel* 11 (2), 537. doi:10.3390/app11020537

Guo, F., Xie, Z. Z., Zhang, N., Zhang, C., Guo, H., Cui, G., et al. (2022). Study on the pore-throat structure characterization and nano grouting law of the low-permeability mudstone based on nmr-rsm methods. *Constr. Build. Mater.* 342, 127913. doi:10.1016/j.conbuildmat.2022.127913

Guo, J. J., Zhang, S. W., Guo, T., and Zhang, P. (2020). Effects of uea and mgo expansive agents on fracture properties of concrete. *Constr. Build. Mater.* 263, 120245. doi:10.1016/j.conbuildmat.2020.120245

He, X., Yang, J. F., Niu, M. D., Zhang, G., and Li, G. (2023). Study on expansion effect and hydration characteristics of ultra-high strength cement-based grouting materials based on humidity compensation. *Case Stud. Constr. Mater.* 18, e01941. doi:10.1016/j.cscm.2023.e01941

Huang, X., Zhao, G., Huang, S., Wang, Z., Wang, X., Tang, C., et al. (2023). Multiscale penetration grouting radius prediction based on geometric characteristics of stacked particles. *Chin. J. Rock Mech. Eng.* 42 (08), 2028–2040. doi:10.13722/j.cnki.jrme.2022.0986

Kang, H., Jiang, P., Huang, B., Guan, X., Wang, Z., Wu, Y., et al. (2020). Roadway strata control technology by means of bolting-modification-destressing in synergy in 1 000 m deep coal mines. *J. China Coal Soc.* 45 (03), 845–864. doi:10.13225/j.cnki.jccs.SJ20.0204

Kang, H. (2021). Seventy years development and prospects of strata control technologies for coal mine roadways in China. *Chin. J. Rock Mech. Eng.* 40 (01), 1–30. doi:10.13722/j.cnki.jrme.2020.0072

Le, H. L., Sun, S. R., Thu, F., and Fan, H. (2019). Experimental investigation on failure modes and mechanical properties of rock-like specimens with a grout-infilled flaw under triaxial compression. *Shock Vib.* 2019, 4909534. doi:10.1155/2019/4909534

Lee, J. S., Bang, C. S., Mok, Y. J., and Joh, S. (2000). Numerical and experimental analysis of penetration grouting in jointed rock masses. *Int. J. rock Mech. Min. Sci.* 37 (7), 1027–1037. doi:10.1016/s1365-1609(00)00040-x

Li, G. Z., Shi, X. S., Gao, Y., Ning, J., Chen, W., Wei, X., et al. (2023). Reinforcing effects of carbon nanotubes on cement-based grouting materials under dynamic impact loading. *Constr. Build. Mater.* 382, 131083. doi:10.1016/j.conbuildmat.2023.131083

Li, Q., Chen, J., Dun, Y., Cao, X., and Liu, Y. (2024). Machine learning based strength prediction method for cement-based grouting material. *J. Hebei Univ. Sci. Technol.* 45(03), 308–317.

Li, S. K., Mo, L. W., Deng, M., and Cheng, S. (2021). Mitigation on the autogenous shrinkage of ultra-high performance concrete via using mgo expansive agent. *Constr. Build. Mater.* 312, 125422. doi:10.1016/j.conbuildmat.2021.125422

Li, Z., Liu, H. X., Dun, Z. L., Ren, L., and Fang, J. (2020). Grouting effect on rock fracture using shear and seepage assessment. *Constr. Build. Mater.* 242, 118131. doi:10.1016/j.conbuildmat.2020.118131

Lin, C. J., Dai, W. J., Li, Z. F., and Wang, Y. (2020). Study on the inorganic synthesis from recycled cement and solid waste gypsum system: application in grouting materials. *Constr. Build. Mater.* 251, 118930. doi:10.1016/j.conbuildmat.2020.118930

Liu, D., Zhao, H., Lin, X., Xiao, C., and Liang, H. Property control of rock fissure sealing material in high altitude cold area. *Water Power* 1-5.

Liu, F. Q., Zheng, M. L., and Ye, Y. S. (2020). Formulation and properties of a newly developed powder geopolymer grouting material. *Constr. Build. Mater.* 258, 120304. doi:10.1016/j.conbuildmat.2020.120304

Liu, Q. S., Lei, G. F., Peng, X. X., Lu, C., and Wei, L. (2018). Rheological characteristics of cement grout and its effect on mechanical properties of a rock fracture. *Rock Mech. rock Eng.* 51 (2), 613–625. doi:10.1007/s00603-017-1340-x

Liu, X. F., Pan, P. Z., Xiong, Z. Q., Zhou, Y. Y., and Wang, Z. F. (2024). Sulfoaluminate cement-based double-liquid material grouting in fractured rock. *Geotech. Lett.* 14 (2), 64–70. doi:10.1680/jgele.24.00016

Lu, C., Wang, J., and Wang, C. Preparation and performance of modified acrylic sand consolidation and water blocking grouting material. *Coal Sci. Technol.*, 1–17.

Lu, H. F., Yin, J. L., Liu, Q. S., Cao, A., Wei, A., and Zhang, K. (2022). A self-dissolved grouting reinforcement method for water-rich soft rock roadway. *Bull. Eng. Geol. Environ.* 81 (7), 256. doi:10.1007/s10064-022-02744-6

Lu, Y. L., Wang, L. G., Li, Z. L., and Sun, H. (2017). Experimental study on the shear behavior of regular sandstone joints filled with cement grout. *Rock Mech. rock Eng.* 50 (5), 1321–1336. doi:10.1007/s00603-016-1154-2

Mu, W. Q., Wang, D. Y., Li, L. C., Yang, T., Feng, Q., Wang, S., et al. (2021). Cement flow in interaction rock fractures and its corresponding new construction process in slope engineering. *Constr. Build. Mater.* 303, 124533. doi:10.1016/j.conbuildmat.2021.124533

Oppong, F., Yao, N., Zhang, W. H., Liu, Y., and Kolawole, O. (2023). Tentative application of expansive cementitious materials in grouting – a systematic review. *Case Stud. Constr. Mater.* 18, e02113. doi:10.1016/j.cscm.2023.e02113

Pan, D. J., Zhang, N., Xiang, Z., and Xie, Z. (2024). Performance improvement of nanocolloidal silica-aluminate cement composite grouting materials with organic acids. *Case Stud. Constr. Mater.* 20, e03166. doi:10.1016/j.cscm.2024.e03166

Qiu, J. D., Huang, R., Wang, H. W., Wang, F., and Zhou, C. (2025). Rate-dependent tensile behaviors of jointed rock masses considering geological conditions using a combined BPM-DFN model: strength, fragmentation and failure modes. *Soil Dyn. Earthq. Eng.* 195, 109393. doi:10.1016/j.soildyn.2025.109393

Qu, X. Z., Shi, X. S., Li, H. X., Ning, J., Li, G., Chen, W., et al. (2024). Enhancement behaviours of carbon nanotubes reinforced cement based grouting materials under dynamic loading. *Case Stud. Constr. Mater.* 21, e03965. doi:10.1016/j.cscm.2024.e03965

Ren, J. L., Zhao, H. B., Zhang, L., Zhao, Z., Xu, Y., Cheng, Y., et al. (2022). Design optimization of cement grouting material based on adaptive boosting algorithm and simplicial homology global optimization. *J. Build. Eng.* 49, 104049. doi:10.1016/j.jobe.2022.104049

Sang, H. M., Liu, B., Liu, Q. S., Kang, Y., and Lu, C. (2024). Study of grouting reinforcement mechanism in fractured rock mass and its engineering application. *Int. J. geomechanics* 24 (5). doi:10.1061/ijgnai.gmeng-9366

Shu, X. J., Zhao, Y., Liu, Z., and Zhao, C. (2022). A study on the mix proportion of fiber-polymer composite reinforced cement-based grouting material. *Constr. Build. Mater.* 328, 127025. doi:10.1016/j.conbuildmat.2022.127025

Sun, Y. T., Li, G. C., Basarir, H., Karrech, A., and Azadi, M. R. (2019). Laboratory evaluation of shear strength properties for cement-based grouted coal mass. *Arabian J. geosciences* 12 (22), 690. doi:10.1007/s12517-019-4908-9

Tan, H. B., Nie, K. J., He, X. Y., Guo, Y., Zhang, X., Deng, X., et al. (2019). Effect of organic alkali on compressive strength and hydration of wet-grinded granulated

blast-furnace slag containing portland cement. *Constr. Build. Mater.* 206, 10–18. doi:10.1016/j.conbuildmat.2019.02.028

Tian, Y. C., Liu, Q. S., Ma, H., and Deng, P. (2018). New peak shear strength model for cement filled rock joints. *Eng. Geol.* 233, 269–280. doi:10.1016/j.enggeo.2017.12.021

Wang, J. J., Wang, Y. L., Yu, J., Xu, L., Li, M., Cheng, J., et al. (2022). Effects of sodium sulfate and potassium sulfate on the properties of calcium sulfoaluminate (csa) cement based grouting materials. *Constr. Build. Mater.* 353, 129045. doi:10.1016/j.conbuildmat.2022.129045

Xu, J. H., Zhang, J. P., li, B. B., Liu, X., Li, K., and Liu, C. (2024). A prestressed anchor-grouting reinforcement method based on the novel hfqsme grouting material for deep high-stress fractured rock mass. *Case Stud. Constr. Mater.* 21, e03889. doi:10.1016/j.cscm.2024.e03889

Zhang, B., Sun, X. M., Yang, K., Guo, P., and Tao, Z. (2022). Model test study on large deformation mechanism of thin-bedded metamorphic sandstone tunnel. *Bull. Eng. Geol. Environ.* 81 (10), 436. doi:10.1007/s10064-022-02937-z

Zhang, J. P., Liu, L. M., and Li, Y. (2023). Mechanism and experiment of self-stress grouting reinforcement for fractured rock mass of underground engineering. *Tunn. Undergr. space Technol.* 131, 104826. doi:10.1016/j.tust.2022.104826

Zhang, W. Q., Zhu, X. X., Xu, S. X., Wang, Z., and Li, W. (2019). Experimental study on properties of a new type of grouting material for the reinforcement of fractured seam floor. *J. Mater. Res. Technol.* 8 (6), 5271–5282. doi:10.1016/j.jmrt.2019.08.049

Zhang, Z. Q., Tian, Z. N., Zhang, K. W., Tang, X., and Luo, Y. (2021). Preparation and characterization of the greener alkali-activated grouting materials based on multi-index optimization. *Constr. Build. Mater.* 269, 121328. doi:10.1016/j.conbuildmat.2020.121328

Zhou, C. T., Rui, Y. C., Qiu, J. D., Wang, Z., Zhou, T., Long, X., et al. (2025). The role of fracture in dynamic tensile responses of fractured rock mass: insight from a particle-based model. *Int. J. Coal Sci. and Technol.* 12, 39. doi:10.1007/s40789-025-00777-2